CARBON 93 (2015) 258–265

Available at www.sciencedirect.com

ScienceDirect

journal homepage: www.elsevier.com/locate/carbon

Composites of MnO_2 nanocrystals and partially graphitized hierarchically porous carbon spheres with improved rate capability for high-performance supercapacitors

Xiaolei Wang [a,1], Xingye Fan [a,1], Ge Li [a], Matthew Li [a], Xingcheng Xiao [b], Aiping Yu [a,*], Zhongwei Chen [a,*]

[a] Department of Chemical Engineering, University of Waterloo, 200 University Avenue West, Waterloo, Ontario N2L3G1, Canada
[b] Chemical Sciences and Materials Systems, General Motors Global Research and Development Center, 30500 Mound Road, Warren, MI 48090, United States

ARTICLE INFO

Article history:
Received 31 January 2015
Accepted 22 May 2015
Available online 27 May 2015

ABSTRACT

Manganese dioxide/carbon nanocomposites with partially graphitized hierarchical porous structure have been designed and synthesized. A high specific capacitance of 412 F g^{-1} and excellent rate capability of these composites can be achieved owing to the interconnected meso- and micro-porous structure and the graphitic pore walls facilitating the ion diffusion and electron transportation, respectively, which is highly demanded for high-performance supercapacitor electrodes materials. Even at a high scan rate of 100 mV s^{-1}, a specific capacitance of 251 F g^{-1} can be obtained, corresponding to 61% capacitance retention. Moreover, a long cycling stability with initial capacitance retention of ~88% is obtained after over 4000 cycles at a current density of 1.0 A g^{-1}. This work presents an efficient electrode materials design and a novel composite which holds great promise in high-performance supercapacitor applications.

1. Introduction

The ever-growing concerns on fossil fuel crisis and ecological deterioration have attracted human beings' attention to the utilization of renewable energies (e.g., tidal, solar, and wind energies) [1]. However, these energies are produced erratically or intermittently, therefore, energy storage, especially electrical energy storage has become one of the essential issues which lead to the better utilization of sustainable energies in the future [2,3]. Among various energy storage technologies, lithium-ion batteries (LIBs) and supercapacitors (SCs) hold great promise in broad applications such as portable electronics, smart grids, and electrical vehicles [4].

Compared to LIBs which have been widely used and possess a high energy density, SCs exhibit much higher power, longer cycling life and shorter charge duration, making them a primary choice in applications where safety and high power are highly required [5–7]. However, SCs often suffer from poor

* Corresponding authors.
E-mail addresses: aipingyu@uwaterloo.ca (A. Yu), zhwchen@uwaterloo.ca (Z. Chen).
[1] These authors contribute equally to this work.
http://dx.doi.org/10.1016/j.carbon.2015.05.072
0008-6223/

energy density, which is determined by the equation $E = 1/2CV^2$, where E is the device energy density, C is the total capacitance, and V is the device working voltage [8]. So far, high surface area carbon-based materials (e.g., activated carbon) have been most commonly used as electrode materials in SCs and can only deliver a specific capacitance of ~150 F g^{-1}, by storing charge on the surface of materials forming an electric double layer [9–12]. Thus, a low energy density (<10 Wh kg^{-1}) is usually obtained. By comparison, pseudocapacitors based on inorganic non-carbon based materials (e.g., RuO_2) store much higher charge (>1000 F g^{-1}) through reversible faradaic reactions [13–17]. Therefore, seeking novel pseudocapacitive materials with high capacitance is one of the key research themes in this field [18].

Among various transition metal oxides, manganese dioxide (MnO_2) has been considered highly promising for SCs, owing to its large reserves in nature, environmental benignity, and a high theoretical capacitance of 1370 F g^{-1} [5,19–24]. In practical applications, however, the performance of MnO_2 is hampered by agglomeration, low electrical conductivity and slow redox rate which is similar to most of other metal oxides, and a low capacitance and a poor rate capability is often observed [25]. To address the above issues, a general strategy is to combine MnO_2 with conductive components [26–28] such as carbon nanotubes (CNTs) [29–31], graphene [32,33], and conductive polymers [34,35]. For example, the conductive polymer wrapped graphene/MnO_2 composite exhibits a high specific capacitance of ~380 F g^{-1} at a current density of 0.1 mA cm^{-2} and ~175 F g^{-1} at 5 mA cm^{-2} [36], while MnO_2/CNT composite material delivers a capacitance of 201 F g^{-1} at a current density of 1.0 A g^{-1} and 140 F g^{-1} at 20 A g^{-1} [37]. Beyond this, it is also important to design and build novel architectures with efficient ion- and electron-transport pathways as well as robustness to further improve the electrode kinetics and integrity, which is highly demanded by high-performance supercapacitors [38,39]. In this context, it is essential but challenging to design and fabricate MnO_2-based electrode materials with novel architectures for high-performance supercapacitors [40–42].

Herein, we report a composite material of MnO_2 nanocrystals/hierarchically porous carbon spheres with partially graphitized surface (MnO_2/C), which exhibits excellent electrochemical performance for asymmetric supercapacitors. Such a composite with unique structure possesses several features favoring high-performance electrodes: (i) the interconnected hierarchically porous structure with micro- and meso-pores not only provides high surface area resulting in high capacitance but also facilitates ion transport leading to high rate capability; (ii) the partially graphitized carbon improves the electron conductivity which further increases high rate capability; (iii) the *in-situ* growth of MnO_2 on carbon spheres ensures an intimate contact between the two components, providing the composites with both high rate and robustness. Moreover, the micrometer-sized composites can be easily fabricated into electrodes by a slurry-coating process compatible with existing battery manufacturing, which makes it a promising material for future practical applications.

2. Experimental

2.1. Synthesis of hierarchically porous graphitized carbon spheres

The hierarchically porous graphitized carbon spheres were synthesized through an aerosol-assisted spray drier (Fig. S1) [43,44]. In a typical synthesis, an homogeneous solution containing sucrose (6.0 g), nickel nitrate (5.0 g), HCl solution (0.1 M, 10 g), distilled de-ionized water (DDI water, 40 mL), tetraethyloxylic silicate (TEOS, 8.0 g) and colloidal silica solution (10 g, LUDOX AS-40) was carried by nitrogen gas and went through an atomizer. The atomizer sprayed the solution in the form of aerosol droplets, which were then sent through drying zone which was heated to 400 °C. Spherical particles formed, induced by solvent evaporating continuously from interface of the air/liquid of the aerosol droplets, and then were collected on a membrane filter before being carbonized at 900 °C under Ar flow. Finally, HCl solution was used to remove the excess of nickel, while NaOH was used to remove the silica template.

2.2. Synthesis of porous and graphitized carbon spheres/MnO_2 composites

The carbon/MnO_2 composites were synthesized by directly reacting $KMnO_4$ with carbon spheres. Briefly, the hierarchically porous graphitized carbon spheres (40 mg) were soaked in Na_2SO_4 solution (0.1 M, 25 mL) for 30 min, and then stirred with an aqueous solution (15 mL) containing Na_2SO_4 (0.1 mol L^{-1}) and $KMnO_4$ (0.1 mol L^{-1}) for various reaction times. The product was washed with DDI water for several times and then dried at 80 °C, and denoted to be MnO_2/C-XX according to different reaction time.

2.3. Materials characterization

Scanning electron microscope (SEM) was used to characterize the morphology of the materials, and was conducted on a LEO FESEM 1530. Transmission electron microscopy (TEM) was used for high resolution imaging, and was performed at the Canadian Center for Electron Microscopy (CCEM, McMaster University), using a JEOL 2010F TEM/STEM field emission microscope. The Nitrogen sorption isotherms were collected from a Micromeritics ASAP 2020 analyzer. The composition was determined by thermal gravimetric analysis (TGA, TA instrument Q500) with a ramp rate of 10 °C min^{-1} from 25 to 850 °C in air. X-ray diffraction (XRD) was performed on PANalytical Empyrean with PIXcel^{3D} detector.

2.4. Electrode fabrication

The electrodes were fabricated from a conventional slurry-coating process. The active material powders, conductive carbon black (Super P carbon) and poly(vinylidene fluoride) were mixed in *N*-methylpyrrolidone (NMP) with a mass ratio of 8:1:1, and then homogenized before being coated on the nickel foam current collectors. The coated electrodes were dried overnight at 100 °C and then pressed at 2.0 MPa. The

mass loading of active materials was controlled to be around 2.0 mg cm^{-2}.

To test electrodes, open cells were assembled using a platinum (Pt) wire as the counter electrode, a SCE reference electrode, and 1 M Na_2SO_4 aqueous solution as the electrolyte. Cyclic voltammetric (CV) and galvanostatic charge–discharge measurements were carried out on a VMP3 potentiostat/galvanostat (Bio-Logic LLC, Knoxville, TN) using cutoff voltages of 1.0 and 0.00 at various scan rates and current densities. The specific capacitance can be calculated based on the equation $C = I/(dE/dt) \approx I/(\Delta E/\Delta t)$, where E is the cell voltage, I is the constant discharge current density, and dE/dt (or $\Delta E/\Delta t$) is the slope of the discharge curve. All electrochemical measurements were carried out at room temperature. The energy density was calculated by $E = (1/2)CV^2$, where E is the energy density, C is the specific discharge capacitance obtained from the galvanostatic charge–discharge curves, and V is the working voltage window. The electrochemical impedance spectroscopy measurement was conducted on a Princeton Applied Research VersaSTAT MC potentiostat. The Nyquist plots were recorded potentiostatically in the frequency ranging from 100 k to 0.01 Hz.

3. Results and discussion

Fig. 1A shows the representative SEM image of as-synthesized porous carbon materials from the aerosol-assisted spray process. The porous carbon possesses a spherical morphology, while the particle size ranges from several hundred nanometers to a few microns, which is much smaller than the activated carbon particles (5–20 μm) commonly used in commercial devices. Fig. 1B shows the representative TEM image of the carbon spheres. The foam-like, highly porous structure can be clearly observed, with meso- and micropores interconnected (Fig. S2). The average mesopore diameter is around 20 nm, which aligns very well with the size of the colloidal silica template particle (~20 nm). To further reveal the unique pore structure of the hierarchically porous carbon spheres, high-resolution TEM was performed. As shown in Fig. 1C, the pore walls of graphitic carbon can be found, suggesting that the carbon material is partially graphitized resulting in significantly improved electron conductivity (Fig. S3). Upon *in-situ* reaction with $KMnO_4$ for 240 min, the spherical morphology and particle size of the MnO_2/C composites can be retained, as shown in Fig. 1D and E, suggesting the successful deposition of MnO_2 nanocrystals (Fig. S4). TEM image (Fig. 1E, inset) of a single MnO_2/C particle indicates that the MnO_2 is uniformly distributed with polycrystalline property (Fig. S5). However, the highly conductive graphitic pore walls still remain, revealed by HRTEM (Fig. 1F, inset), suggesting that the $KMnO_4$ preferably reacts with amorphous carbon, which ensures the efficient electron transfer pathways.

The successful *in-situ* growth of MnO_2 was further confirmed by X-ray photoelectron spectroscopy (XPS). The obtained XPS survey spectrum (Fig. S6A) presents the signals from Mn, O, and C elements, suggesting the existence of manganese oxide on porous carbon materials. Fig. 2A shows the core-leveled scan of Mn $2p_{3/2}$ and Mn $2p_{1/2}$ with binding energies at 642.5 and 654.1 eV, respectively. Both the binding energies and the spin energy of 11.6 eV are consistent with literatures reported previously, confirming the formation of

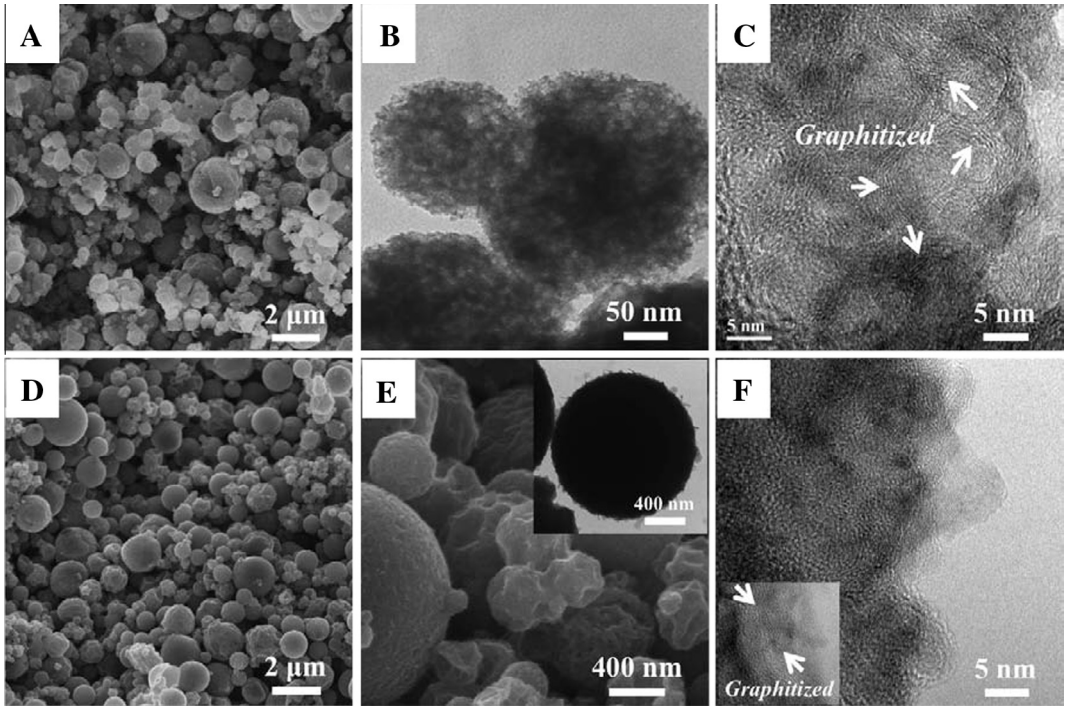

Fig. 1 – (A) SEM, (B) TEM, and (C) high-resolution TEM images of as-synthesized hierarchically porous carbon spheres; (D) low and (E) high magnification SEM images of the MnO_2/C composite particles with a reaction time of 240 min. Inset: a TEM image of a single MnO_2/C particle; (F) high-resolution TEM image of part of the MnO_2/C composite particle.

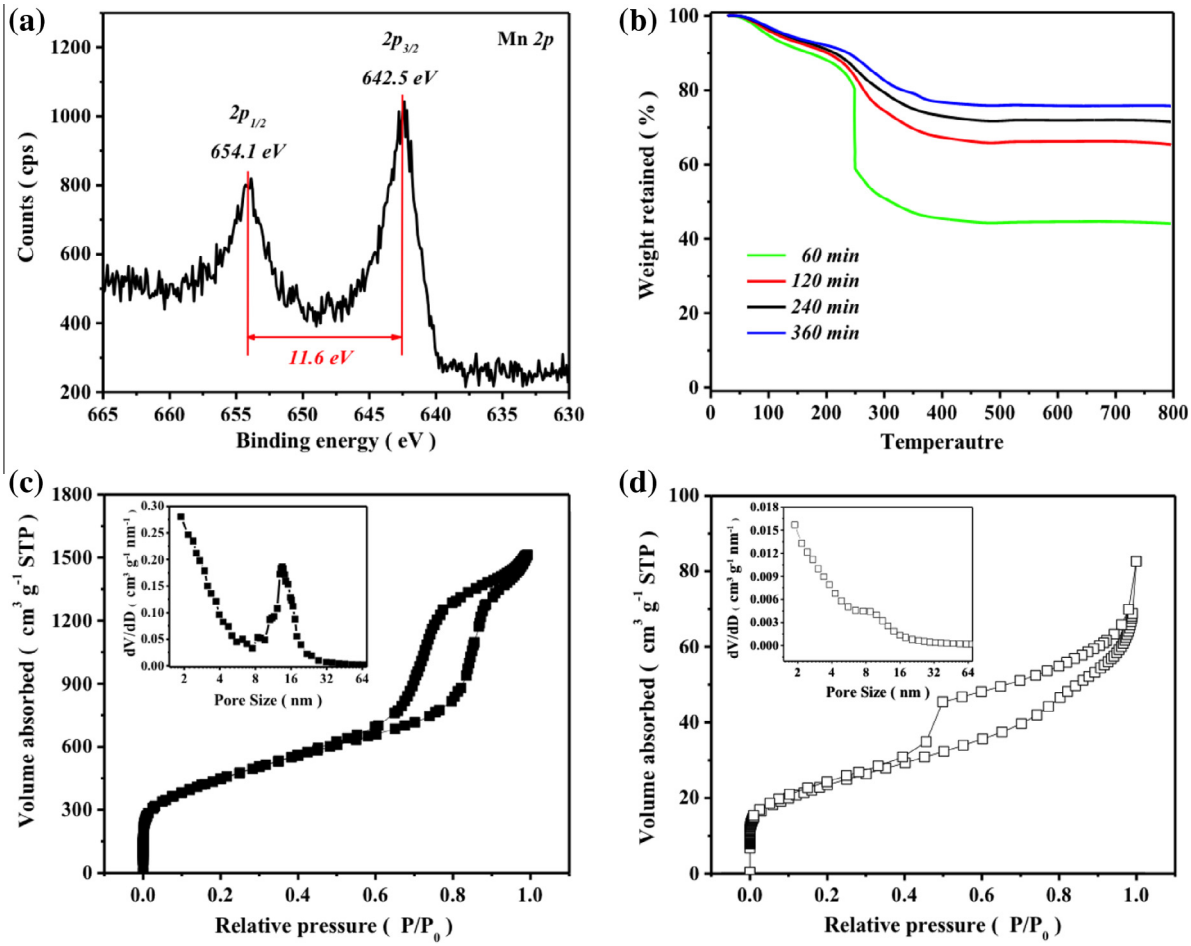

Fig. 2 – (A) Core-leveled scan Mn $2p_{3/2}$ and Mn $2p_{1/2}$ XPS spectra of MnO_2/C composites; (B) thermogravimetric analysis (TGA) curves of MnO_2/C composites synthesized at different reaction times; nitrogen adsorption/desorption isotherms and size distributions of (C) as-synthesized hierarchically porous carbon spheres, and (D) MnO_2/C-240 composites. (A color version of this figure can be viewed online.)

MnO_2 [45,46]. The X-ray diffraction pattern of the MnO_2/C composites can be indexed to JCPDS card No. 02-1070 (Fig. S6B), indicating a hydrate form of the crystal MnO_2. The *d*-spacing is calculated to be 0.24 nm, which is highly consistent with HRTEM observation. The amount of MnO_2 grown on porous carbon can be controlled by adjusting the reaction time of $KMnO_4$ with carbon spheres substrates. Fig. 2B shows the thermogravimetric analysis (TGA) curves of MnO_2/C composites with different reaction times, where three main regions can be observed. Below 200 °C, a gradual mass decrease is found, mainly due to the removal of moistures, some remaining hydroxyl- or carboxyl-groups on the carbon materials, and the structural water as observed from XRD result. The sharp mass loss below 400 °C is ascribed to the consumption of carbon catalyzed by MnO_2 and its derivatives [47]. Above 500 °C, no obvious weight loss can be observed. All carbon materials are consumed completely, while MnO_2 is transformed to thermodynamically stable Mn_2O_3. The final weight percentage was calculated to be 44%, 65%, 72%, and 76% for reaction time of 60, 120, 240, and 360 min, corresponding to MnO_2 content of 49%, 72%, 79%, and 84% in composites (Fig. S7). The large content of MnO_2 in our composite materials is mainly attributed to the hierarchical structure of the carbon substrates, which provides large surface area and fast permanganate ion diffusion channels.

The pore structure of MnO_2/C composites was analyzed by nitrogen adsorption/desorption technique. The nitrogen adsorption/desorption isotherms and pore size distribution of as-synthesized hierarchically porous carbon is shown in Fig. 2C. A type-IV isotherm is obtained with nitrogen uptakes at relative pressure below 0.2 and between 0.6 and 0.9, respectively, suggesting that micropores and mesopores coexist. The pore size centers at ~14 nm and below 2 nm (Fig. 2C, inset), which further confirms the hierarchically porous structure. The size of the mesopores is a little smaller than the silica colloidal templates, which is mainly attributed to the Ni catalysis induced graphitization process. The hierarchically porous carbon spheres possess a high Brunauer–Emmett–Teller (BET) surface area of 1173 $m^2 g^{-1}$ with a high pore volume of 2.46 $cm^3 g^{-1}$. By comparison, the MnO_2/C-240 also exhibits a type-IV isotherm (Fig. 2D), but a lower BET surface area of ~100 $m^2 g^{-1}$ and a decreased mesopore size of ~9 nm (Fig. 2D, inset), suggesting the successful and homogeneous

growth of MnO_2. However, the hierarchically porous structure still exists with interconnected micro- and meso-pores, which facilitates the ion transportation.

The electrochemical properties of as-synthesized hierarchically porous carbon and MnO_2/C composites were firstly characterized by cyclic voltammetry (CV) in a three electrode open cell using Na_2SO_4 solution as the electrolyte, a Pt wire as the counter electrode and SCE reference electrode. Fig. 3A shows the typical CV curves of as-synthesized hierarchically porous carbon. A nearly symmetrical rectangular shape can be observed from all CV curves at various scan rates, corresponding to the electrical double-layer capacitance where all charge stores on the surface of the materials. The rectangular shape remains as scan rate increases, owing to the connected pores and excellent conductivity stemming from the partially graphitized carbon. By comparison, MnO_2/C-240 electrode also exhibits symmetric rectangular shaped CV curves, suggesting fast reversible Faradic reactions and ideal capacitive performance. However, an obvious distortion occurs as the scan rate increases, indicating the polarization resulting from the increased transport resistance.

The specific capacitance can be calculated from CV curve. Fig. 3C compares the specific capacitance of as-synthesized hierarchically porous carbon and MnO_2/C-240 calculated from CV curves at different scan rates of 2–100 mV s^{-1} (corresponding to the charge/discharge times from 500 to 10 s). Obviously, the hierarchically porous carbon electrode exhibits a high rate capability with a low capacitance of 91 F g^{-1} from electrical double-layer capacitance. In contrast, the MnO_2/C-240 electrode possesses a much higher capacitance of 412 F g^{-1} at a scan rate of 2 mV s^{-1}. Such a high specific capacitance is mainly ascribed to the high MnO_2 ratio in the composites, which has seldom been reported previously. Even at high scan rate of 50 and 100 mV s^{-1}, the composite electrode still delivers a high capacitance of 286 and 251 F g^{-1}, respectively, which is 70% and 61% of the capacitance at 2 mV s^{-1}. Such an observation indicates a much improved rate performance of pseudocapacitive metal oxides mainly attributed to the unique hierarchically porous structure and the highly conductive graphitic pore walls. Fig. 3D further compares the rate capability of MnO_2/C composites with different MnO_2 ratios. It can be found that the rate performance deteriorates as the MnO_2 content increases. For low MnO_2 ratio, the composite electrode gives a good rate capability but a low specific capacitance (Fig. S8) due to the limited contribution from pseudocapacitance. For high MnO_2 ratio, although the

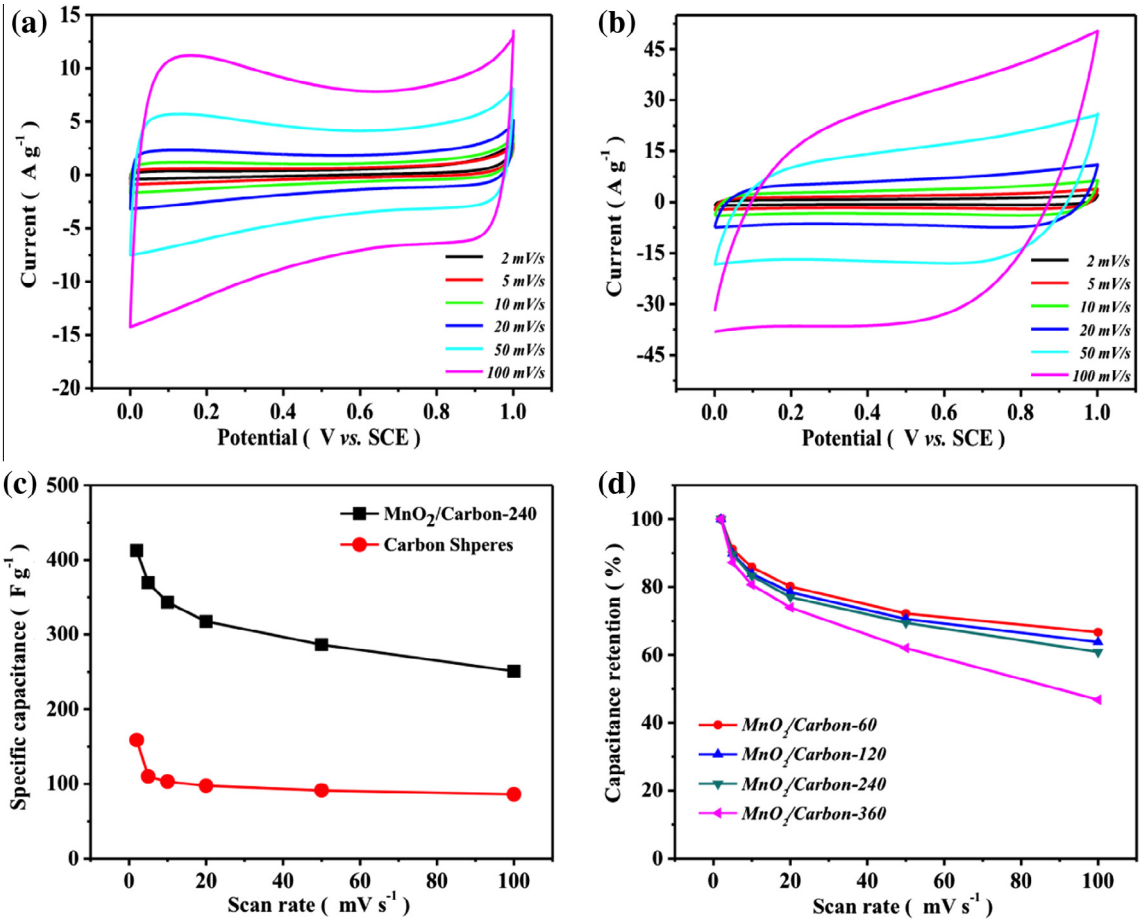

Fig. 3 – Cyclic voltammograms of (A) as-synthesized hierarchically porous carbon spheres, and (B) MnO_2/C-240 at various scan rates from 2 to 100 mV s^{-1} at a cutting-off voltage of 1.0 and 0.0 V *vs.* SCE; (C) comparison of specific capacitance dependence on scan rates for both as-synthesized hierarchically porous carbon spheres and MnO_2/C-240; and (D) comparison of rate capability of MnO_2/C composites with different MnO_2 contents. (A color version of this figure can be viewed online.)

composite electrode delivers a much higher capacitance at low scan rate, the rate capability is compromised (Fig. S8). On the one hand, the *in-situ* growth of MnO_2 on porous carbon with long reaction time results in the collapse of hierarchical pores and the interconnected channels, and the loss of highly conductive graphitic carbon part, which significantly affects the ion- and electron-transportation. On the other hand, the formation of MnO_2 leads to less specific surface area and pore volume, which also increases the diffusion resistance. Therefore, an optimal MnO_2 ratio where both high capacitance and rate capability can be obtained is highly needed.

The rate capability of MnO_2/carbon composites (MnO_2/C-240) were further compared with that of a series of MnO_2/porous carbon composites including MnO_2/hierarchically porous carbon [48], MnO_2/graphitic disordered mesoporous carbon [49], MnO_2/CMK-3 [42], and mesoporous MnO_2/carbon aerogel [26]. As shown in Fig. 4A, the MnO_2/carbon from this work outperforms most of the others. Although mesoporous MnO_2/carbon aerogel shows a little higher capacitance at low scan rate, its deteriorative capacitance retention at higher scan rates is unsatisfactory. In order to further evaluate the capacitive behavior of MnO_2/C composites, galvanostatic charge–discharge measurements were applied at various current densities. Fig. 4B shows the galvanostatic charge–discharge profiles of MnO_2/C-240 electrode at current densities from 0.5 to 5.0 A g^{-1} between 1.0 and 0.0 V (*vs.* SCE). Symmetrical charge and discharge profiles can be obtained, suggesting typical and excellent capacitive property of the composites, which is consistent with CV observations. The specific capacitance derived from the discharge curve is calculated to be 328 F g^{-1} at a current density of 0.5 A g^{-1} (discharging time: 656 s); while at 5.0 A g^{-1}, the MnO_2/C-240 electrode still possesses a discharge capacitance of 266 F g^{-1} (discharging time: 52 s).

The corresponding rate performance is clearly observed from Fig. 4C. At the current density of 5.0 A g^{-1}, the MnO_2/C-240 electrode still possesses ~81% of its specific capacitance at 0.5 A g^{-1}. This performance is much better than that of MnO_2/graphitic carbon spheres [50] and hierarchically MnO_2/carbon nanocomposites [51]. As we mentioned above, this excellent rate capability is mainly attributed to the highly conductive graphitic pore walls. As shown in Raman spectrum, two peaks can be easily found at 1327 (D band) and 1588 (G band) cm^{-1} with a relative intensity ratio (I_D/I_G) of 1.48, which confirms that a large amount of graphitized carbon exists (Fig. S9). Even after the MnO_2 deposition, the two peaks can still be observed with an I_D/I_G of 1.50, suggesting that $KMnO_4$ preferably reacts with amorphous carbon,

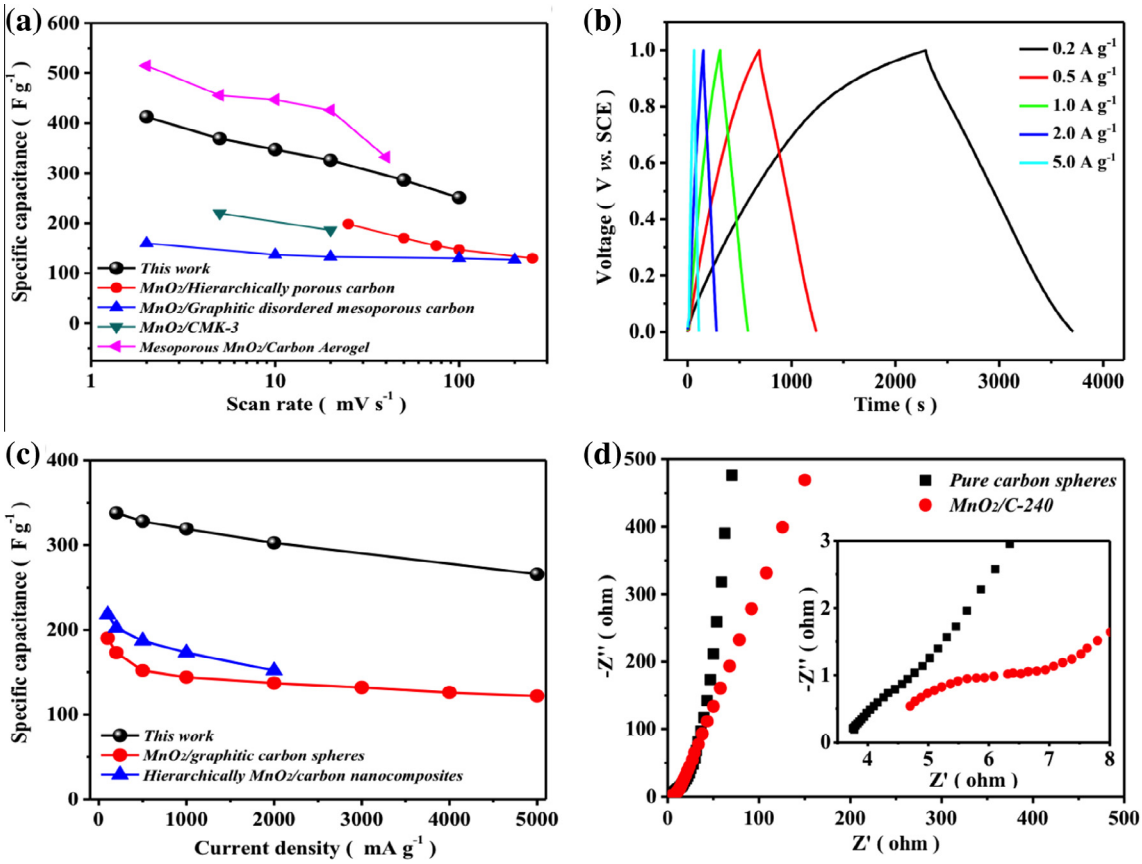

Fig. 4 – (A) Comparison of specific capacitance of MnO_2/C-240 dependence on scan rates with a series of MnO_2/porous carbon composites; (B) galvanostatic charge–discharge profiles of MnO_2/C-240 with the cut-off voltage of 1.0 and 0.0 V *vs.* SCE at various current densities ranging from 0.2 to 5.0 A g^{-1}; and (C) corresponding specific capacitance dependence on current densities; and (D) comparison of Nyquist plots of as-synthesized hierarchically porous carbon spheres and MnO_2/C-240. (A color version of this figure can be viewed online.)

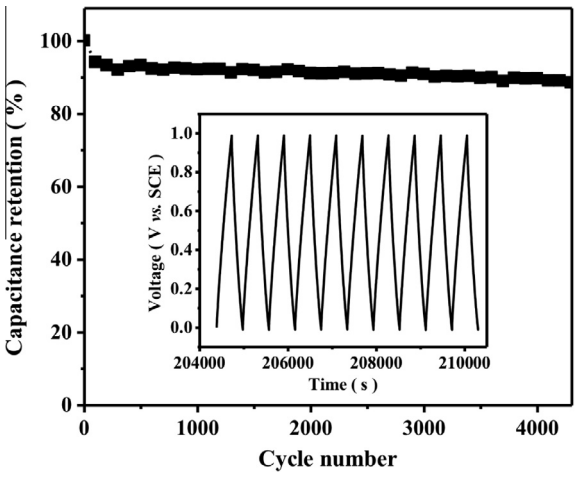

Fig. 5 – Long-term cycling stability of MnO_2/C-240 composite electrode at a current density of 1.0 A g^{-1} for over 4000 cycles.

leaving highly conductive graphitized carbon which facilitates the electron transfer.

Such a good performance can be further confirmed by electrochemical impedance spectroscopy (EIS) result. As shown in Fig. 4D, each Nyquist plot is composed of a semicircle at high-frequency region representing the resistance of electrolyte and charge-transfer, and a Warburg tail at low-frequency region representing the diffusion-resistance from the electrode materials. Obviously, as-synthesized hierarchically porous carbon spheres exhibit a high conductivity according to the small semicircle and low slope of the Warburg tail. Remarkably, the MnO_2/C-240 shows a comparable conductivity, which is mainly due to the *in-situ* growth of MnO_2 on highly conductive networks formed within the carbon spheres.

In addition to the excellent rate capability, a long cycling stability of the MnO_2/C composites can be also achieved. Cycling life test over 4000 cycles for MnO_2/C-240 electrode was carried out at 1.0 A g^{-1}, and the corresponding normalized capacitance retention is shown in Fig. 5. After 4300 cycles, the MnO_2/C-240 electrode still possesses ~88% of its initial specific capacitance with very symmetric and stable charge–discharge profiles. Such a cycling stability is mainly attributed to the robust composite structure. On the one hand, the unique graphitic pore walls serve as a robust scaffold preventing the porous structure from collapse. On the other hand, the growth of MnO_2 from *in-situ* reaction of $KMnO_4$ with carbon materials ensures an intimate contact, where MnO_2 and carbon are firmly connected. Moreover, the hierarchically porous framework can effectively suppress the MnO_2 from aggregation.

4. Conclusion

We have successfully designed and synthesized MnO_2/partially graphitized carbon spheres composites that can provide fast ion-diffusion and electron-transfer channels for supercapacitor applications. The composites electrodes exhibit both excellent rate capability and long cycling stability due to the unique hierarchical porous structure, the graphitic pore walls, and the *in-situ* reaction between $KMnO_4$ and carbon spheres. Such a novel design and facile synthesis provides a promising path for material and electrode design in practical supercapacitor applications.

Acknowledgments

This work was supported by the Natural Sciences and Engineering Research Council of Canada (NSERC), the University of Waterloo, and the Waterloo Institute for Nanotechnology.

Appendix A. Supplementary data

Supplementary data associated with this article can be found, in the online version, at http://dx.doi.org/10.1016/j.carbon.2015.05.072.

REFERENCES

[1] Armand M, Tarascon JM. Building better batteries. Nature 2008;451(7179):652–7.
[2] Dell RM, Rand DAJ. Energy storage-a key technology for global energy sustainability. J Power Sources 2001;100(1–2):2–17.
[3] Arico AS, Bruce P, Scrosati B, Tarascon J-M, van Schalkwijk W. Nanostructured materials for advanced energy conversion and storage devices. Nat Mater 2005;4(5):366–77.
[4] Winter M, Brodd RJ. What are batteries, fuel cells, and supercapacitors? Chem Rev 2004;104(10):4245–70.
[5] Simon P, Gogotsi Y. Materials for electrochemical capacitors. Nat Mater 2008;7(11):845–54.
[6] Conway BE. Electrochemical supercapacitors: scientific fundamentals and technological applications. New York: Kluwer Academic/Plenum Publishers; 1999. p. 29.
[7] Simon P, Gogotsi Y, Dunn B. Where do batteries end and supercapacitors begin? Sci Mag 2014;343:1201–11.
[8] Zheng JP. The limitations of energy density of battery/double-layer capacitor asymmetric cells. J Electrochem Soc 2003;150(4):A484–92.
[9] Zhang LL, Zhao XS. Carbon-based materials as supercapacitor electrodes. Chem Soc Rev 2009;38(9):2520–31.
[10] Jiang H, Lee PS, Li C. 3D carbon based nanostructures for advanced supercapacitors. Energy Environ Sci 2013;6(1):41–53.
[11] Dai Y, Jiang H, Hu Y, Fu Y, Li C. Controlled synthesis of ultrathin hollow mesoporous carbon nanospheres for supercapacitor applications. Ind Eng Chem Res 2014;53(8):3125–30.
[12] Zhu Z, Hu Y, Jiang H, Li C. A three-dimensional ordered mesoporous carbon/carbon nanotubes nanocomposites for supercapacitors. J Power Sources 2014;246:402–8.
[13] Augustyn V, Come J, Lowe MA, Kim JW, Taberna P-L, Tolbert SH, et al. High-rate electrochemical energy storage through Li+ intercalation pseudocapacitance. Nat Mater 2013;12(6):518–22.
[14] Augustyn V, Simon P, Dunn B. Pseudocapacitive oxide materials for high-rate electrochemical energy storage. Energy Environ Sci 2014;7(5):1597–614.
[15] Conway BE. Transition from "supercapacitor" to "battery" behavior in electrochemical energy storage. J Electrochem Soc 1991;138(6):1539–48.
[16] Yan Y, Cheng Q, Zhu Z, Pavlinek V, Saha P, Li C. Controlled synthesis of hierarchical polyaniline nanowires/ordered

bimodal mesoporous carbon nanocomposites with high surface area for supercapacitor electrodes. J Power Sources 2013;240:544–50.
[17] Yan Y, Cheng Q, Wang G, Li C. Growth of polyaniline nanowhiskers on mesoporous carbon for supercapacitor application. J Power Sources 2011;196(18):7835–40.
[18] Jiang H, Ma J, Li C. Mesoporous carbon incorporated metal oxide nanomaterials as supercapacitor electrodes. Adv Mater 2012;24(30):4197–202.
[19] Whittingham MS. Materials challenges facing electrical energy storage. MRS Bull 2008;33(04):411–9.
[20] Wu Z-S, Ren W, Wang D-W, Li F, Liu B, Cheng H-M. High-energy MnO_2 nanowire/graphene and graphene asymmetric electrochemical capacitors. ACS Nano 2010;4(10):5835–42.
[21] Qu Q, Zhang P, Wang B, Chen Y, Tian S, Wu Y, et al. Electrochemical performance of MnO_2 nanorods in neutral aqueous electrolytes as a cathode for asymmetric supercapacitors. J Phys Chem C 2009;113(31):14020–7.
[22] Xu C, Kang F, Li B, Du H. Recent progress on manganese dioxide based supercapacitors. J Mater Res 2010;25(08):1421–32.
[23] Wei W, Cui X, Chen W, Ivey DG. Manganese oxide-based materials as electrochemical supercapacitor electrodes. Chem Soc Rev 2011;40(3):1697–721.
[24] Jiang H, Dai Y, Hu Y, Chen W, Li C. Nanostructured ternary nanocomposite of rGO/CNTs/MnO_2 for high-rate supercapacitors. ACS Sustain Chem Eng 2014;2(1):70–4.
[25] Liu C, Li F, Ma L-P, Cheng H-M. Advanced materials for energy storage. Adv Mater 2010;22(8):E28–62.
[26] Li G-R, Feng Z-P, Ou Y-N, Wu D, Fu R, Tong Y-X. Mesoporous MnO_2/carbon aerogel composites as promising electrode materials for high-performance supercapacitors. Langmuir 2010;26(4):2209–13.
[27] Yuan L, Lu X-H, Xiao X, Zhai T, Dai J, Zhang F, et al. Flexible solid-state supercapacitors based on carbon nanoparticles/MnO_2 nanorods hybrid structure. ACS Nano 2011;6(1):656–61.
[28] Chen S, Zhu J, Wu X, Han Q, Wang X. Graphene oxide–MnO_2 nanocomposites for supercapacitors. ACS Nano 2010;4(5):2822–30.
[29] Jiang H, Li C, Sun T, Ma J. A green and high energy density asymmetric supercapacitor based on ultrathin MnO_2 nanostructures and functional mesoporous carbon nanotube electrodes. Nanoscale 2012;4(3):807–12.
[30] Chou S-L, Wang J-Z, Chew S-Y, Liu H-K, Dou S-X. Electrodeposition of MnO_2 nanowires on carbon nanotube paper as free-standing, flexible electrode for supercapacitors. Electrochem Commun 2008;10(11):1724–7.
[31] Hu L, Chen W, Xie X, Liu N, Yang Y, Wu H, et al. Symmetrical MnO2-carbon nanotube-textile nanostructures for wearable pseudocapacitors with high mass loading. ACS Nano 2011;5(11):8904–13.
[32] Fan Z, Yan J, Wei T, Zhi L, Ning G, Li T, et al. Asymmetric supercapacitors based on graphene/MnO_2 and activated carbon nanofiber electrodes with high power and energy density. Adv Funct Mater 2011;21(12):2366–75.
[33] Li Z, Mi Y, Liu X, Liu S, Yang S, Wang J. Flexible graphene/MnO_2 composite papers for supercapacitor electrodes. J Mater Chem 2011;21(38):14706–11.
[34] Prasad KR, Miura N. Polyaniline-MnO_2 composite electrode for high energy density electrochemical capacitor. Electrochem Solid-State Lett 2004;7(11):A425–8.
[35] Sharma RK, Rastogi AC, Desu SB. Manganese oxide embedded polypyrrole nanocomposites for electrochemical supercapacitor. Electrochim Acta 2008;53(26):7690–5.
[36] Yu G, Hu L, Liu N, Wang H, Vosgueritchian M, Yang Y, et al. Enhancing the supercapacitor performance of graphene/MnO_2 nanostructured electrodes by conductive wrapping. Nano Lett 2011;11(10):4438–42.
[37] Li L, Hu ZA, An N, Yang YY, Li ZM, Wu HY. Facile synthesis of MnO_2/CNTs composite for supercapacitor electrodes with long cycle stability. J Phys Chem C 2014;118(40):22865–72.
[38] Long JW, Dunn B, Rolison DR, White HS. Three-dimensional battery architectures. Chem Rev 2004;104(10):4463–92.
[39] Fischer AE, Pettigrew KA, Rolison DR, Stroud RM, Long JW. Incorporation of homogeneous, nanoscale MnO_2 within ultraporous carbon structures via self-limiting electroless deposition: implications for electrochemical capacitors. Nano Lett 2007;7(2):281–6.
[40] Li H, Jiang L, Cheng Q, He Y, Pavlinek V, Saha P, et al. MnO_2 nanoflakes/hierarchical porous carbon nanocomposites for high-performance supercapacitor electrodes. Electrochim Acta 2015;164:252–9.
[41] Liu M, Gan L, Xiong W, Xu Z, Zhu D, Chen L. Development of MnO_2/porous carbon microspheres with a partially graphitic structure for high performance supercapacitor electrodes. J Mater Chem A 2014;2(8):2555–62.
[42] Dong X, Shen W, Gu J, Xiong L, Zhu Y, Li H, et al. MnO_2-embedded-in-mesoporous-carbon-wall structure for use as electrochemical capacitors. J Phys Chem B 2006;110(12):6015–9.
[43] Chen Z, Wen J, Yan C, Rice L, Sohn H, Shen M, et al. High-performance supercapacitors based on hierarchically porous graphite particles. Adv Energy Mater 2011;1(4):551–6.
[44] Lu Y, Fan H, Stump A, Ward TL, Rieker T, Brinker CJ. Aerosol-assisted self-assembly of mesostructured spherical nanoparticles. Nature 1999;398(6724):223–6.
[45] Wang J-G, Yang Y, Huang Z-H, Kang F. Rational synthesis of MnO_2/conducting polypyrrole@carbon nanofiber triaxial nano-cables for high-performance supercapacitors. J Mater Chem 2012;22(33):16943–9.
[46] Chen H, Dong X, Shi J, Zhao J, Hua Z, Gao J, et al. Templated synthesis of hierarchically porous manganese oxide with a crystalline nanorod framework and its high electrochemical performance. J Mater Chem 2007;17(9):855–60.
[47] Shen B, Qinlei. Study on MSW catalytic combustion by TGA. Energy Convers Manage 2006;47(11–12):1429–37.
[48] Chou T-c, Doong R-a, Hu C-c, Zhang B, Su DS. Hierarchically porous carbon with manganese oxides as highly efficient electrode for asymmetric supercapacitors. ChemSusChem 2014;7(3):841–7.
[49] Patel MN, Wang X, Slanac DA, Ferrer DA, Dai S, Johnston KP, et al. High pseudocapacitance of MnO_2 nanoparticles in graphitic disordered mesoporous carbon at high scan rates. J Mater Chem 2012;22(7):3160–9.
[50] Lei Z, Zhang J, Zhao XS. Ultrathin MnO_2 nanofibers grown on graphitic carbon spheres as high-performance asymmetric supercapacitor electrodes. J Mater Chem 2012;22(1):153–60.
[51] Peng Y, Chen Z, Wen J, Xiao Q, Weng D, He S, et al. Hierarchical manganese oxide/carbon nanocomposites for supercapacitor electrodes. Nano Res 2011;4(2):216–25.